Int. J. Solids Structures Vol. 15, pp. 55–71

0020-7683/79/0101-0055/$02.00/0

A NUMERICAL ANALYSIS OF VOID GROWTH IN TENSION CREEP

M. A. BURKE† and W. D. NIX‡

Department of Materials Science and Engineering, Stanford University, Stanford, CA 94305, U.S.A.

(*Received* 30 *January* 1978; *in revised form* 7 *June* 1978; *received for publication* 1 *August* 1978)

Abstract—The uniaxial creep deformation of a material containing a doubly periodic square array of circular cylindrical voids is studied under plane strain conditions. A variational principle for incompressible nonlinear viscous behavior is used as the basis for implementing a finite element solution. The effects of large, time dependent deformation are included in the formulation. A power law creep relationship is used and results are obtained for the influence of different stress exponents on the overall ductility. The void shape evolution and zones of concentrated deformation are described under increasing overall strain.

1. INTRODUCTION

Fracture of polycrystalline solids under creep conditions typically occurs by the growth and coalescence of microscopic voids that form in the grain boundaries[1–3]. The corresponding ductility is often very low, even for metals and alloys that are quite ductile at room temperature. Most of the theories that have been developed for intergranular fracture at elevated temperatures are based on the premise that voids grow by the absorption of vacancies[4–8]. It is known that a sufficient number of vacancies can be generated in the grain boundaries and transported by diffusion to the growing voids. The rate of void growth can be obtained by solving the diffusion boundary value problem associated with a model for growth by vacancy absorption. Following this approach, a related expression for the time to rupture, t_r, invariably exhibits a reciprocal dependence on the applied stress ($t_r \sim \sigma^{-1}$)[5]. However, it is often observed that t_r is actually proportional to σ^{-m} where $m > 1.0$ (typically $3 \leq m \leq 50$[9–12]). If mechanisms for void nucleation are included in the analysis, values of $m > 1.0$ can be derived, but close correlation with experiments is rare[13]. Furthermore, these same experimental results, which pertain to the power law regime of creep, indicate that this value of m frequently corresponds to the stress exponent, n, in the expression $\dot{\epsilon}_{SS} = \beta\sigma^n$ [14–16]. Here $\dot{\epsilon}_{SS}$ is the steady state or minimum creep rate in the typical three stage (primary, steady state, tertiary) description of creep deformation. In addition, the temperature dependences for both creep and fracture are almost always related. These observations were made first by Monkman and Grant[14] who suggested that creep fracture occurs when $\dot{\epsilon}_{SS} t_r = C$, where C is a constant. This is known as the Monkman–Grant relation, with C being a measure of creep ductility.

The validity of this empirical relation implies that steady state creep dominates the creep process and suggests that the mechanism for fracture is closely linked to creep itself. A number of other experimental observations also support the view that vacancy diffusion to the void surface may not be the rate controlling mechanism in cavity growth.

It has been found that the rate of cavity growth for an alloy is markedly lower than that for the pure material under the same creep conditions, even though the alloy additions do not change the diffusion coefficients substantially. Furthermore, the decrease in cavity growth rate on alloying is comparable with the observed decrease in creep rate[17, 18].

The fact that there is an apparent relationship between the creep and rupture processes ($m = n$), leads to the conjecture that if creep fracture occurs by void growth, then the growth is dominated by the mechanism for creep itself. Hence, void growth might be attributed to the inhomogeneous plastic deformation of the surrounding grains. A model for creep fracture can then be developed in the context of continuum plasticity. This is the approach which has been taken in the study of the ductile rupture of time independent elastic–plastic materials[19–21].

Any model for high temperature integranular fracture based on the growth of voids by creep

†Formerly Graduate Research Assistant at Stanford, now Senior Engineer at Marc Analysis Research Corporation, Palo Alto, CA 94306, U.S.A.

‡Professor of Materials Science and Engineering at Stanford.

inherently contains the apparent connection between deformation and rupture time. The predictions of the model would be automatically consistent with the form of the Monkman–Grant relation, although the value of the constant C would be predicted only if the model includes the dominant features of the actual physical situation[22]. To begin the development of a comprehensive description of creep fracture, the relation between the growth of a void and remotely imposed uniform stress and strain rate fields must be found. An important aspect of this treatment is the extent to which voids interact, or, alternatively, the extent to which the triaxial stress state resulting from void interactions contributes to void coalescence[23]. This aspect has already been considered in the study of void growth in materials with time independent plastic behavior. These studies[19–21], for the most part, have not considered interaction effects *per se* as only single isolated voids are treated. However, they show clearly that finite fracture strains can be predicted only when a void lies in the neighborhood of other voids even though the far field stress state is one of simple tension.

The purpose of the present study is to examine the influence of void interaction on ductility when the material behavior is time dependent plastic in nature and is described by the steady state power law creep relation. A particular void growth boundary value problem is considered in which a stress triaxiality is provided by void interactions. It is the nonlinearly viscous analog to the time independent elastic–plastic analysis performed by Needleman[24]. Specifically it is the study of the creep deformation of a doubly periodic array of cylindrical voids under the action of a uniaxially applied displacement rate. The particular creep rupture model which is considered serves mainly to demonstrate the capability of a computational scheme to analyze inhomogeneous creep deformation and to give some initial insight into the development of a more realistic model for intergranular fracture.

In the following sections a variational principle is described for strictly incompressible viscous flow. A discretization of the principle is shown which is suitable for nonlinear material behavior and finite deformation. The results of the void growth study are then presented.

2. A VARIATIONAL PRINCIPLE FOR CREEP

Finite element formulations for the analysis of time dependent plastic deformation have, for the most part, been restricted to the study of infinitesimal deformation[25–27]. The deformation is considered to be elastic-time dependent plastic in nature. The plastic component of strain is treated in a pseudo-elastic fashion. These so-called initial strain formulations are subject to numerical instability in the computational procedure[28]. For this reason only small increments of plastic deformation can be taken in each step and therefore the analysis of finite time dependent deformation by this method is not practical. A more productive approach to the analysis of finite creep deformation can be made if elastic effects are neglected.

The field equations which govern steady state creep are given below. For equilibrium we have

$$\sigma_{ij,j} + X_i = 0, \tag{1}$$

where σ_{ij} are the stress components. It is assumed that inertial effects for creeping flow can be neglected and that the body force term, X_i, is only a function of position. For incompressibility we write

$$\dot{u}_{i,i} = 0, \tag{2}$$

where $\dot{u}_i$ is the ith component of displacement rate. The constitutive relation may be written as

$$\sigma_{ij} = -p\delta_{ij} + 2\mu\dot{\epsilon}_{ij}, \tag{3}$$

where μ is the viscosity coefficient, $p = -\sigma_{kk}/3$, and $\dot{\epsilon}_{ij} = \dot{\epsilon}'_{ij}$ when eqn (2) is satisfied. Also

$$\dot{\epsilon}_{ij} = \frac{1}{2}(\dot{u}_{i,j} + \dot{u}_{j,i}). \tag{4}$$

The current configuration is chosen as the reference state in which the material is considered to occupy the volume V, bounded by the surface S over a portion of which, $S_{\bar{T}}$, surface tractions, $\bar{T}_i$, are prescribed and a complementary portion, $S_{\bar{u}}$, over which displacement rates, $\bar{u}$, are prescribed. Hence

and
$$\sigma_{ij}n_j = \bar{T}_i \qquad \text{on } S_{\bar{T}}, \tag{5}$$

$$\dot{u}_i = \bar{\dot{u}}_i \qquad \text{on } S_{\bar{u}} \tag{6}$$

It follows from eqns (1) and (3) that

$$\sigma_{ij,j} = -p_{,i} + \mu\dot{u}_{i,jj}. \tag{7}$$

A solution is sought for a velocity field which makes stationary a functional and which satisfies prescribed velocity boundary conditions (eqn 6). The Euler equations must be the field equations governing the response of the material. A suitable functional is the rate form of the potential energy

$$I = \int_V \sigma_{ij}\dot{\epsilon}_{ij}\,\mathrm{d}V - \int_{S_{\bar{T}}} \bar{T}_i\dot{u}_i\,\mathrm{d}S - \int_V X_i\dot{u}_i\,\mathrm{d}V, \tag{8}$$

or

$$I = \int_V \sigma_{ij}\dot{\epsilon}_{ij}\,\mathrm{d}V - \int_V p\dot{\epsilon}_{ii}\,\mathrm{d}V - \int_{S_{\bar{T}}} \bar{T}_i\dot{u}_i\,\mathrm{d}S - \int_V X_i\dot{u}_i\,\mathrm{d}V, \tag{9}$$

where again use has been made of the fact that $\dot{\epsilon}'_{ij} = \dot{\epsilon}_{ij}$ for strictly incompressible plastic flow. The first tems on the r.h.s. of the above expression represents the rate of dissipation of internal energy. The second term serves to enforce a constraint on the admissible velocity fields to only incompressible deformation. The hydrostatic pressure, p, acts as a Lagrangian multiplier and is not derivable from the velocity field. The latter terms in eqn (9) represent the rate of change of external work done on the system. The functional is a function of both the velocity and pressure fields. Hence, a hybrid formulation is required. When the functional is made stationary then the first variation with respect to all variables is zero,

$$\delta_{\dot{u}_i,p} I = 0. \tag{10}$$

The Euler equations corresponding to variations in the velocity field are therefore

$$\mu(\dot{u}_{i,jj} + \dot{u}_{j,ij}) - p_{,i} + X_i = 0, \tag{11}$$

and for variations in the hydrostatic pressure field

$$\dot{u}_{i,i} = 0. \tag{12}$$

Substituting eqn (12) into eqn (11) yields

$$\mu\dot{u}_{i,jj} - p_{,i} + X_i = 0. \tag{13}$$

Hence, equilibrium and incompressibility are identically satisfied when this functional is made stationary.

The specific functions, $\dot{u}_i$ and p, which give rise to a stationary value of I, are obtained from the solution of

$$\delta I = \int_V \sigma'_{ij}\delta\dot{\epsilon}_{ij}\,\mathrm{d}V - \int_V \delta p\dot{\epsilon}_{ii}\,\mathrm{d}V - \int_V p\delta\dot{\epsilon}_{ii}\,\mathrm{d}V - \int_{S_{\bar{T}}} \bar{T}_i\delta\dot{u}_i\,\mathrm{d}S - \int_V X_i\delta\dot{u}_i\,\mathrm{d}V = 0, \tag{14}$$

where variations with respect to displacement rates imply corresponding variations in strain rate according to the linear strain rate-velocity relationship (eqn 4).

If the hydrostatic pressure variable is transformed to h, where

$$h = -\frac{p}{\mu} = \frac{\sigma_{kk}/3}{\mu}, \tag{15}$$

and the deviatoric components of stress are expressed in terms of strain rate, the variational equality is given as

$$\delta I = \int_V 2\mu\dot{\epsilon}_{ij}\delta\dot{\epsilon}_{ij}\,dV + \int_V h\mu\delta\dot{\epsilon}_{ii}\,dV + \int_V \mu\dot{\epsilon}_{ii}\delta h\,dV - \int_{S_{\bar{T}}} \bar{T}_i\delta\dot{u}_i\,dS - \int_V X_i\delta\dot{u}_i\,dV = 0. \tag{16}$$

The solution to the boundary value problem, to be discussed subsequently, will be obtained by a discretization of eqn (16). Nonlinear viscous incompressible deformation can be treated by solving this equation in an iterative manner.

3. A FINITE ELEMENT DISCRETIZATION

The components of displacement rate at a generic point (x_1, x_2) are described in an approximate manner according to the finite element method of analysis by the relationship

$$\{\dot{u}(x_1, x_2)\} = [N_{\dot{u}}(x_1, x_2)]\{\dot{U}\}. \tag{17}$$

Here, $\{\dot{U}\}$ is the vector of nodal point displacement rates and $[N_{\dot{u}}]$ is the matrix of interpolating functions which are associated with each of the nodes. Similarly, the hydrostatic function can be approximated by the relationship

$$h(x_1, x_2) = [N_h(x_1, x_2)]\{H\}. \tag{18}$$

A different set of interpolating functions is chosen to describe the pressure distribution. The reason for this will be described subsequently. It follows from eqn (17) and the definition of the rate of deformation that

$$\{\dot{\epsilon}(x_1, x_2)\} = [N'_{\dot{u}}]\{\dot{U}\}, \tag{19}$$

where

$$\{\dot{\epsilon}\}^T = [\dot{\epsilon}_{xx} \quad \dot{\epsilon}_{yy} \quad 2\dot{\epsilon}_{xy}]. \tag{20}$$

Also,

$$[N'_{\dot{u}}(x_1, x_2)] = [L][N_{\dot{u}}] \tag{21}$$

where $[L]$ is a differential operator matrix which takes the form

$$[L] = \begin{bmatrix} \partial/\partial x & 0 \\ 0 & \partial/\partial y \\ \partial/\partial y & \partial/\partial x \end{bmatrix}, \tag{22}$$

for planar deformation.

The rate of dilatation can also be expressed in terms of nodal point displacement rates by the relationship

$$\dot{\epsilon}_{ii}(x_i, x_2) = \{M\}^T\{\dot{\epsilon}\} = \{M\}^T[N'_{\dot{u}}]\{\dot{U}\}, \tag{23}$$

where

$$\{M\}^T = [1 \quad 1 \quad 0]. \tag{24}$$

A discrete form for the variation of the potential energy can be obtained by substitution of the above matrix terms into eqn (16). Hence,

$$\delta I = \{\delta\dot{U}\}^T\left[\left(\int_V [N'_{\dot{u}}]^T[c][N'_{\dot{u}}]\,dV\right)\cdot\{\dot{U}\} + \left(\int_V [N'_{\dot{u}}]^T\{M\}\mu[N_h]\,dV\right)\cdot\{H\} - \int_{S_{\bar{T}}}[N_{\dot{u}}]^T\{\bar{T}\}\,dS\right] + \{\delta H\}^T\left[\left(\int_v [N_h]^T\mu\{M\}^T[N_{\dot{u}}]\,dV\right)\cdot\{\dot{U}\}\right] = 0, \quad (25)$$

where

$$[c] = \begin{bmatrix} 2\mu & 0 & 0 \\ 0 & 2\mu & 0 \\ 0 & 0 & \mu \end{bmatrix}. \quad (26)$$

The body force term which appears in eqn (16) has been omitted at this stage as it is not required for the boundary value problems which will be considered here. Since eqn (25) must hold for any admissible and independent variations of the displacement rates or the hydrostatic variables, then each of the bracketed terms appearing in this expression must be equal to zero. A set of simultaneous algebraic equations can then be developed to solve for the discrete values of the unknowns. The integral expressions appearing as coefficients in the variational equality can be evaluated by virtue of the characteristics ascribed to a finite element or region. The solution is then obtained from the following set of equations

$$\sum_{i=1}^{N_e}\left\{\left[\int_{V_i}([N'_{\dot{u}}]_i^T[c][N'_{\dot{u}}]_i + [N_h]_i^T\cdot\mu\cdot[N'_{\dot{u}}]_i)\,dV_i\right]\cdot\{\dot{U}\}_i + \left(\int_{V_i}[N'_{\dot{u}}]_i^T\{M\}^T\cdot\mu\cdot[N_h]_i\,dV_i\right)\cdot\{H\}_i\right\} = \sum_{j=1}^{N_s}\int_{S_j}[N_{\dot{u}}^k]_j^T\{\bar{T}\}\,dS_j, \quad (27)$$

where subscripts i and j refer to a particular element. The total number of elements is N_e and N_s is the number of elements with a surface, S_j, along that portion of the boundary, $S_{\bar{T}}$, where tractions are prescribed. The superscript k refers to the subset of interpolating functions for element j that is associated with nodal points along the traction boundary. Since eqn (27) contains first order derivatives of the displacement rate, the interpolative description for this variable must be continuous across inter-element boundaries. Continuity of higher order derivatives of the displacement rate, the pressure function, and its derivatives is not required. This condition will just be satisfied by employing a linear approximation for the displacement rate field and by allowing the pressure function to be a constant over the region of one element.

For this particular study an eight node isoparametric element was used. Hence, the components of displacement rate are described within an element by the following

$$\dot{u}_i(\xi,\eta) = \sum_{j=1}^{8} N_j(\xi,\eta)\dot{U}_i^j, \qquad i = 1,2 \quad (28)$$

where (ξ,η) are the normalized coordinates of the element. Equation (28) provides a higher order polynomial approximation of the displacement rate than that required for continuity but it is a convenient representation when consideration is given to the functional form of the pressure distribution.

The proper functional form of the hydrostatic pressure variable can be determined by considering the last term in eqn (25) which can now be written as

$$\sum_{i=1}^{N_e}\int_{V_i}\{\delta H\}_i^T[N_h]_i^T\cdot\mu\cdot\{M\}^T[N'_{\dot{u}}]_i\{\dot{U}\}_i\,dV_i = 0. \quad (29)$$

These equations represent the constraint on the allowable displacement rates which enforces incompressibility. The latter part of the integrand

$$\{M\}^T[N'_{ii}]_i\{\dot{U}\}_i = \dot{\epsilon}_{ii}(x_1, x_2)_i, \tag{30}$$

is a polynomial expression for the rate of dilatation throughout element i. The remaining terms in the integrand

$$\{\delta H\}_i^T[N_h]_i^T \cdot \mu = \delta p(x_1, x_2)_i, \tag{31}$$

represent a polynomial approximation for the variation in hydrostatic pressure throughout the element in terms of the nodal point values of the pressure function. If the description of the pressure function is taken as a constant throughout one element then the integrand of eqn (29) reduces to

$$\delta p_i \int_{V_i} \{M\}^T[N'_{ii}]_i\{\dot{U}\}_i \, dV. \tag{32}$$

If this quantity is identically zero for all variations, δp_i, then the integrand itself must be equal to zero and the total volume of an element will remain unchanged. However, it cannot be inferred that the condition of pointwise incompressibility has been met. If a higher order polynomial approximation is taken for the pressure field, then each coefficient in the resulting polynomial

$$\delta p_i(x_1, x_2)\dot{\epsilon}_{ii}(x_1, x_2)$$

is dependent upon the particular values chosen for the components of $\{\delta H\}_i$. This expression cannot be identically equal to zero for any $\{\delta H\}_i$ unless the polynomial expression for $\dot{\epsilon}_{ii}$ is zero at all points within the element. The degree of the polynomial which describes the pressure function determines the number of nodal point values that are associated with each element, and correspondingly, the number of constraint equations associated with the nodal point displacement rates. A degree of polynomial must therefore be chosen that does not overly constrain the displacement rates but does provide the closest approximation to pointwise incompressibility. A polynomial for $h(x_1, x_2)$ was chosen which had the same degree as that for $\dot{\epsilon}_{ii}(x_1, x_2)$. This was accomplished by using the interpolating functions associated with a 4 node isoparametric element, the next lower order element in the family of isoparametric quadrilateral elements to the 8 node element used for the displacement rate field and the geometric description. Discrete values of the hydrostatic pressure function were assigned to the corner nodes of the 8 node element. A dummy pressure function value was also assigned to each of the mid-side nodes. The associated interpolating function had a null value. This facilitated the formation of the element stiffness matrix and the assembly of the overall set of equations as each node had three degrees of freedom and could be treated in sequence equally.

If the element nodal point variables are grouped in the following manner

$$\{\varphi\}_i^T = [\dot{U}_1^1, \dot{U}_2^1, H^1, \ldots \dot{U}_1^8, \dot{U}_2^8, H^8]_i, \tag{33}$$

then eqn (27) can be written in the standard form as

$$\left(\sum_{i=1}^{N_e}[K_i]\{\varphi\}\right) = \sum_{j=1}^{N_s}\{\bar{F}_j\}, \tag{34}$$

where

$$[K_i] = \int_{V_i}[N_T]^T[D][N_T] \, dV_i. \tag{35}$$

The matrix $[N_T]$ is a partitioned matrix consisting of terms from both $[N_{\dot{u}}]$ and $[N_h]$ such that

$$\left\{\frac{\dot{\epsilon}}{\dot{h}}\right\} = [N_T]\{\varphi\}. \tag{36}$$

The matrix $[D]$ has the form:

$$[D] = \begin{bmatrix} 2\mu & 0 & 0 & \mu \\ 0 & 2\mu & 0 & \mu \\ 0 & 0 & \mu & 0 \\ \mu & \mu & 0 & 0 \end{bmatrix} \tag{37}$$

It will be a function of position when the material behavior is nonlinear viscous.

4. THE VOID GROWTH PROBLEM

The specific problem studied is the overall tensile deformation of a doubly periodic square array of cylindrical voids as shown in Fig. 1. Plane strain deformation is considered in the plane perpendicular to the cylinder axes ($\dot{\epsilon}_{33} = 0$). The initial radius of the void is R_0 and the initial distance between centers of the circles is $2L_0$. The array is imagined to be divided into square cells of side $2L_0$, with one void centered in each cell. By virtue of the dictated symmetry of the deformation of the array, the behavior of only one quadrant of one cell need be studied. The boundary value problem associated with this region is illustrated in Fig. 2 for the configuration at $t = 0$. For convenience and without loss of generality, the displacement rate $\dot{u}_2$ is taken to be zero along the x_1 axis and the displacement rate $\dot{u}_1$ is taken to be zero along the x_2 axis. The boundary conditions along the x_1 axis are therefore

$$\dot{u}_2(x_1, 0) = 0 \tag{38a}$$

$$\bar{T}_1(x_1, 0) = 0 \tag{38b}$$

and

$$\dot{u}_1(0, x_2) = 0 \tag{38c}$$

$$\bar{T}_2(0, x_2) = 0 \tag{38d}$$

along the x_2 axis. The boundary condition at the void interface is

$$\bar{T}_i = 0, \qquad i = 1, 2. \tag{38e}$$

On the top face of the cell, $x_2 = L_0$, the boundary conditions are

$$\dot{u}_2(x_1, L_0) = \dot{V} \tag{38f}$$

$$\bar{T}_1(x_1, L_0) = 0 \tag{38g}$$

where $\dot{V}$ is the prescribed displacement rate. On the side of the cell $x_1 = L_0$,

$$\bar{T}_2(L_0, x_2) = 0 \tag{38h}$$

$$\dot{u}_1(L_0, x_2) = \dot{W} \tag{38i}$$

where $\dot{W}$ is independent of x_2 and is determined by the condition of no constraint in the x_1 direction, which is

$$\int_0^{L_0} T_1(L_0, x_2)\, dx_2 = 0. \tag{38j}$$

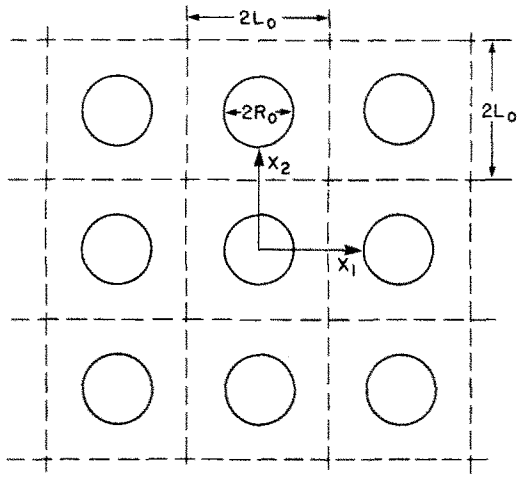

Fig. 1. A creep fracture model—the doubly periodic array of voids.

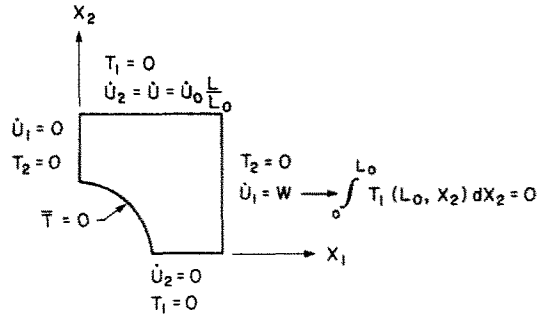

Fig. 2. A void cell quadrant—the displacement rate boundary value problem for void growth.

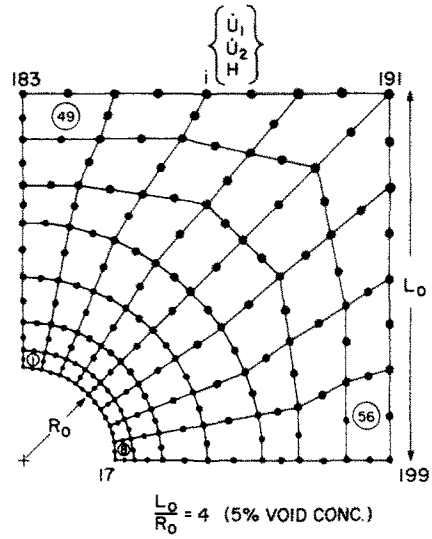

Fig. 3. The finite element mesh used to describe deformation of the void cell quadrant.

A cell quadrant is discretized in the manner illustrated in Fig. 3. The unknown displacement rates and pressure function values can be obtained by solving the matrix equation

$$[A]\{\varphi\} = \{F\} \tag{39}$$

where $[A]$ is the assembled summation of element stiffness matrices. The vector $\{F\}$ is derived from the displacement rate boundary condition (38f). The void growth boundary condition (38i) is satisfied by assigning the same degree of freedom number, 432, which is associated with the

x_1 component of the displacement rate of node 199 (Fig. 3) to the x_1 components of nodes 191–198. Column 432 of the [A] matrix then extended beyond the band of nonzero coefficients associated with the normal connectivity of this mesh. The terms lying above the band were stored separately to avoid the storage of an excessive number of zero coefficients and a standard Gauss elimination procedure for solution of the matrix equation was modified to account for these terms.

5. CONSTITUTIVE BEHAVIOR

The solution of the matrix equation (39) must be obtained in an iterative manner due to the nonlinear nature of the material response. It was assumed that the creep relationship can be generalized, by means of the von Mises criterion to describe nonlinear viscous behavior for multiaxial stress states. Hence, the effective strain rate is given by

$$\dot{\bar{\epsilon}} = \beta \bar{\sigma}^n \tag{40}$$

where

$$\dot{\bar{\epsilon}} = \sqrt{\left(\frac{2}{3}\dot{\epsilon}_{ij}\dot{\epsilon}_{ij}\right)} \tag{41}$$

and, the effective stress is obtained from

$$\bar{\sigma} = \sqrt{\left(\frac{3}{2}\sigma'_{ij}\sigma'_{ij}\right)}. \tag{42}$$

The explicit form of the constitutive relationship for steady state creep behavior is then given by

$$\sigma_{ij} = 2\left[\frac{1}{3\beta^{1/n}}\dot{\bar{\epsilon}}^{(1-n)/n}\right]\dot{\epsilon}_{ij}. \tag{43}$$

The viscosity coefficient, therefore, is given by

$$\mu = \frac{1}{3\beta^{1/n}}\dot{\bar{\epsilon}}^{(1-n)/n}. \tag{44}$$

So, for other than linearly viscous behavior ($n = 1$), it can be deduced from eqns (19), (36), (41) and (44) that

$$\mu = f(\varphi) \tag{45}$$

and eqn (39) is now

$$[A(\varphi)]\{\varphi\} = \{F(t)\}. \tag{46}$$

The load vector is denoted as a function of time because the prescribed x_2 component of nodal displacement rate along the top face of the cell was varied with each increment of deformation so as to maintain a constant overall strain rate, $\dot{\epsilon}_{22}$, in that direction, i.e.

$$\dot{V} = L_2\dot{\epsilon}_{22} \tag{47}$$

where L_2 is the current length of the cell.

During any step, r, in the iterative scheme, unless convergence has occurred, eqn (46) will not be satisfied by the rth solution, $\{\varphi\}_r$. A system of residual forces, $\{R(\varphi)\}_r$, will exist such that

$$\{R(\varphi)\}_r = [A(\varphi)]_r\{\varphi\}_r - \{F\}. \tag{48}$$

The iterative procedure which was used in this study was one of successive substitutions of previous solutions, $\{\varphi\}_r$, into the reformulation of the current assembly matrix. This technique which is the simplest to apply also exhibited a reasonable rate of convergence. Iteration was terminated when

$$(\varphi_i^r - \varphi_i^{r-1})/\varphi_i^r < 1\%, \qquad i = 1, \ldots n.$$

Some further saving in computation was realized in the reformulation of the assembly matrix at each iteration step by retaining the matrices $[N_T(\xi_k, \eta_l)]$ and the coordinate Jacobians $|J(\xi_k, \eta_l)|$. The matrices $[D(\xi_k, \eta_l)]$ can then be readily computed from eqns (36), (41) and (44). The element stiffness matrices then follow from (35). Convergence was also accelerated in some instances by assuming as an initial guess for the solution at a particular step an extrapolation of the solutions at two preceding steps.

6. DISCRETIZATION

The initial solution for a particular value of the creep exponent, n, was found by first obtaining the linear viscous solution ($n = 1$) where μ and $[A]$ are not dependent on the unknown variables. Solutions were then obtained for successive values of n ($t = 0$) using the iterative procedure until the required value was reached. The deformation was traced incrementally by updating the corner nodal point coordinates after a convergent solution was obtained for a particular configuration, i.e.

$$X_i^j \to X_i^j + \dot{U}_i^j \Delta t.$$

The time increment, Δt, was adjusted continuously to permit only small increments of deformation. Also, at certain stages in the overall deformation of the cell, a new mesh was defined so as to redistribute elements and focus them in regions where the strain rate gradients were large.

7. RESULTS

The principal objective of the analysis of the void growth problem is to determine quantitatively the influence of the creep stress exponent on the overall ductility of a material containing voids. A single cell/void size ratio was used corresponding to approximately a 5% volume concentration of voids ($L_0/R_0 = 4/1$). A series of four tests was performed with values of the creep exponent, n, equal to 1, 2, 5 and 10. The magnitude of the creep constant, β, was fixed at 10^{-19} [(psi)^n sec]$^{-1}$ and the constant uniaxially applied strain rate, ϵ_{22}, was fixed at 0.25×10^{-14} sec^{-1}. The numerical results describe the evolution of the void shape and the redistribution of the stress and strain rate fields with overall deformation.

The shape evolution of the void, as illustrated in Fig. 4 for the case $n = 5$, typifies the results for the series. The circular cross section becomes essentially elliptical under the action of a uniaxially applied strain rate. Initially the void surface contracts laterally but at a slower rate than for a single void in an infinite medium subjected to the same far field strain rate. This is due to the attractive interaction effect of the laterally adjacent void. The lateral distance between the voids decreases despite void contraction since the cell itself is contracting at a faster rate at this stage. Essentially a condition of plastic instability develops when the lateral distance becomes sufficiently reduced ($U/L_0 = 0.4$ in Fig. 4).

The ligament between the void surface and the lateral cell boundary begins to behave in a manner similar to the necked region of a tensile test specimen at the point where deviation from apparent uniform deformation occurs [29]. The lateral displacement of the void surface reverses direction and the voids coalesce at an accelerated rate ($U/L_0 = 0.95$). This rate is strongly related to the creep stress exponent of the material. Creep fracture becomes imminent at this point.

The configuration of one quadrant of a unit void cell, following the initial increments of deformation is schematically represented in Fig. 5. The material behavior here is linearly viscous. Hence, the stress distribution will be identical to that for plane strain linear elastic deformation which is incompressible. The configuration of an imaginary unit cell of the same dimensions which surrounds a single void in an infinite medium is also shown. The solutions for

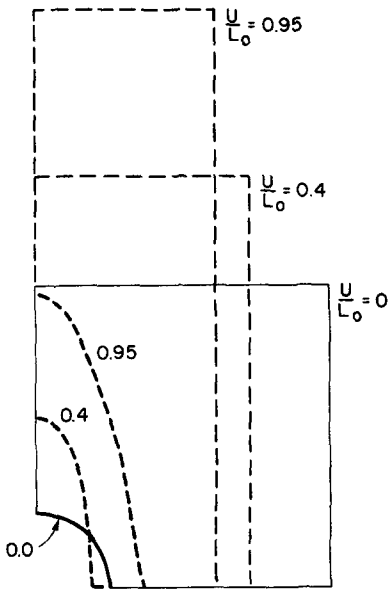

Fig. 4.

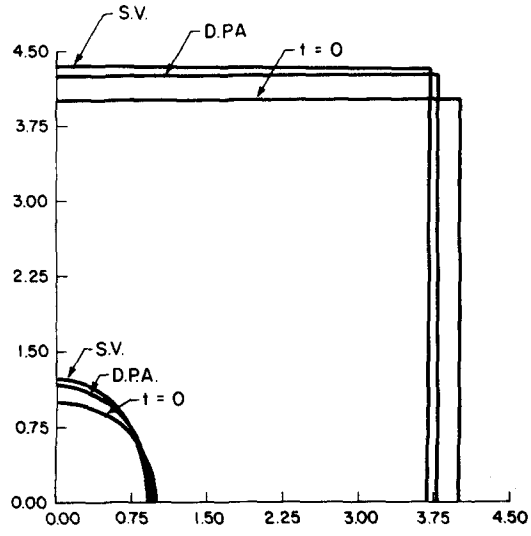

Fig. 5.

Fig. 4. Shape evolution of a void cell quadrant during creep ($L_0/R_0 = 4$, $n = 5$).

Fig. 5. Initial displacement. Single void (S.V.) vs doubly periodic array (D.P.A.)—$L_0/R_0 = 4$, $n = 1$.

the stress and displacement rate field are known in the case of the isolated void[30]. In the absence of adjacent void interactions, the deformation in the vicinity of the void is greater, particularly in the regions along the x_1 and x_2 axes. The radial components of displacement rate at the void surface were evaluated as -0.25×10^{-14} and 0.75×10^{-14} along the x_1 and x_2 axes respectively. The corresponding values for the doubly periodic array were computed as -0.1965×10^{-14} and 0.6539×10^{-14} or approximately 80% of the above values.

The initial ($t = 0$) stress distribution for linearly viscous behavior is illustrated in Fig. 6 for both the doubly periodic array and the single void geometry. The stress concentration factor at the void surface is 3.0 for the single void and approximately 2.66 for the array. The lateral void

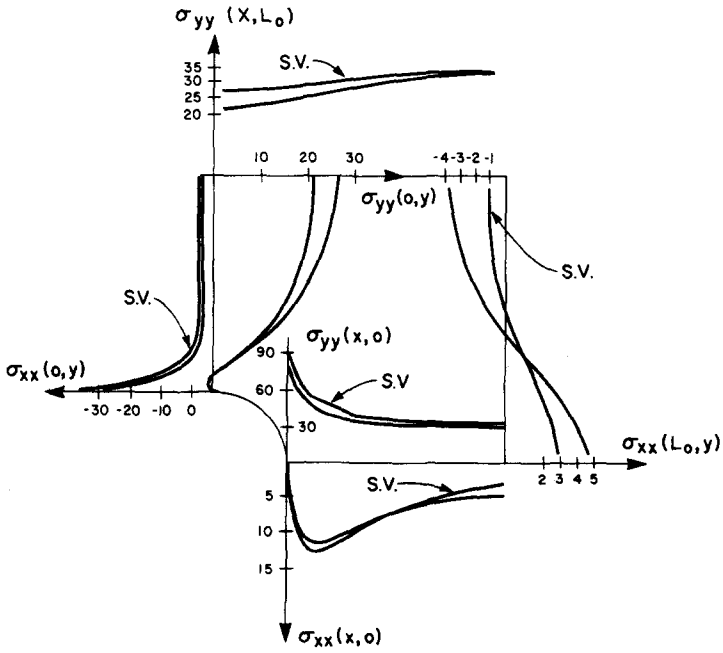

Fig. 6. Initial stress state (K.S.I.) single void (S.V.) vs doubly periodic array ($L_0/R_0 = 4$, $n = 1$).

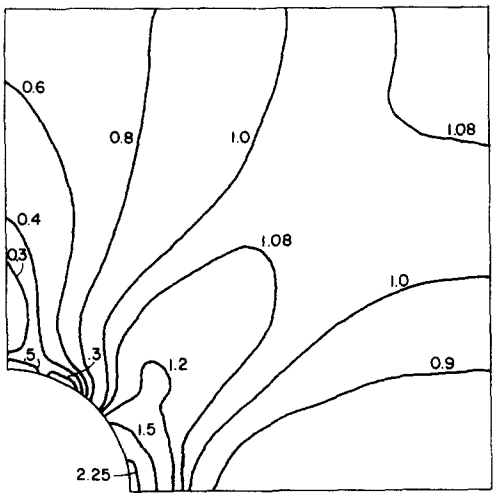

Fig. 7. Effective strain rate contours, $\dot{\bar{\epsilon}}/\dot{\bar{\epsilon}}_0$. Doubly periodic array—uniaxially applied displacement rate ($L_0/R_0 = 4$, $n = 1$, $t = 0.0$).

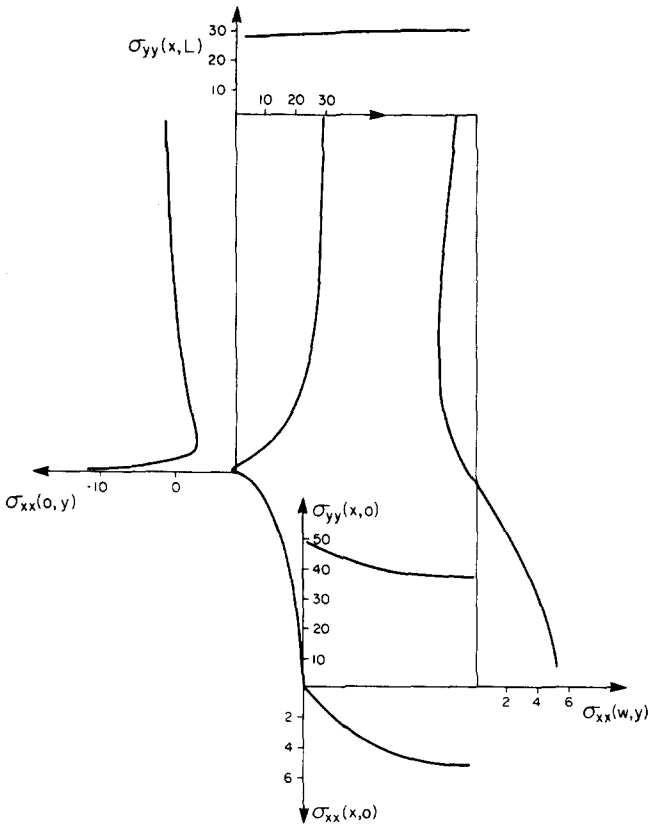

Fig. 8. Stress distribution (K.S.I.) doubly periodic array—constant overall strain rate in y-direction ($L_0/R_0 = 4$, $n = 1$, $U/L_0 = 0.5707$).

interaction is reflected in larger values of the transverse component of stress (σ_{11}) near the cell boundary for the array. The net zero traction condition (38j) along the unit cell boundary is satisfied by the σ_{11} distribution shown in Fig. 6.

Effective strain rate contours were derived using eqns (36) and (41). The results for linearly viscous behavior in the initial configuration are illustrated in Fig. 7. The effective strain rate values shown here and in subsequent figures have been normalized with respect to the effective strain rate of material with the same viscous behavior deforming with the same applied strain

rate, but containing no voids. The pattern was found to be typical for all values of the creep exponent. It can be noted that the largest concentration of deformation occurs in the region of the void surface nearest the x_1 axis. To a lesser extent, deformation is concentrated along the diagonal which intersects the void and the r.h.s. of the cell. A third region of moderately concentrated deformation lies at the void surface nearest the x_2 axis where a state of triaxial compression exists. The stress distribution in the unit cell with linear viscous behavior is illustrated in Fig. 8 for a subsequent stage of deformation ($U/L_0 = 0.5707$). As deformation proceeds, the ligament between the void surface and the cell boundary assumes a gradual necked shape. At $U/L_0 = 0.5707$, the distribution of σ_{22} along the x_1 axis is approaching the uniform value $\sigma_{22} = L_1/D_1 \cdot S'$, where L_1, D_1 are the widths of the cell and ligament respectively. Here, S' is the current nominal stress needed to accommodate a constant overall strain rate for the array. By examining σ_{22} along the top of the cell in Fig. 8 it appears that S' is approx. 29,000 psi at this stage, or 87% of the nominal tensile stress value for the pure material or single void case.

The effective strain rate contours for the cell at the point $U/L_0 = 0.5707$ are illustrated in Fig. 9 ($n = 1$). The next level of creep exponent which was considered was for the case $n = 2$. The effective strain rate contours ($t = 0$) are shown in Fig. 10. The magnitudes of those contours in the critical region near the void surface and along the cell diagonal are greater and the values in other regions are less than for the linear case.

The contours are also shown when $U/L_0 = 0.70075$ ($n = 2$) in Fig. 11. The lateral displacement of the void surface has already reversed direction ($U/L_0 = 0.5575$) and the strain rate is becoming more uniform at any section through the lower portion of the ligament. The maximum strain rate concentration factor at the void surface has decreased from 3.4 ($t = 0$) to 1.58 ($U/L_0 = 0.70075$).

The results for the test with a creep exponent equal to five are illustrated in Figs. 12 and 13.

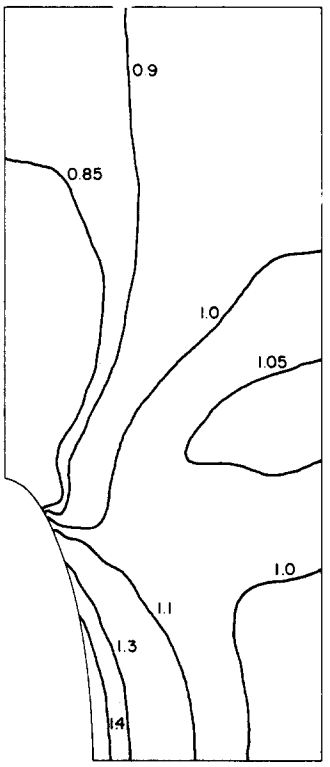

Fig. 9.

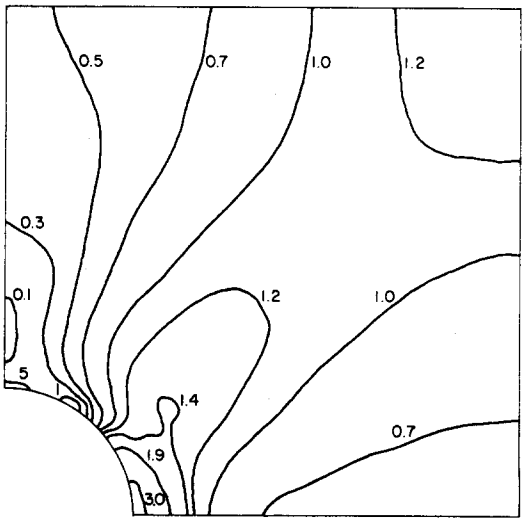

Fig. 10.

Fig. 9. Effective strain rate contours, $\dot{\bar{\epsilon}}/\dot{\bar{\epsilon}}_0$. Doubly periodic array—constant uniaxially applied overall strain rate ($L_0/R_0 = 4$, $n = 1$, $U/L_0 = 0.5707$).

Fig. 10. Effective strain rate contours, $\dot{\bar{\epsilon}}/\dot{\bar{\epsilon}}_0$. Doubly periodic array—uniaxially applied displacement rate ($L_0/R_0 = 4$, $n = 2$, $t = 0.0$).

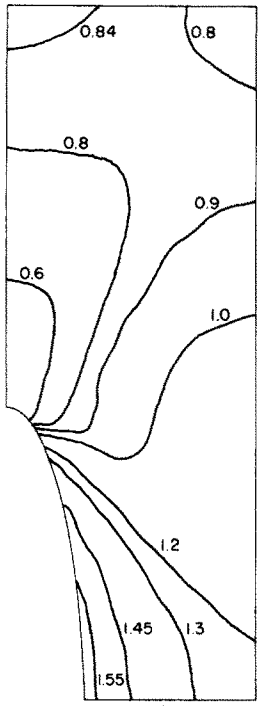

Fig. 11.

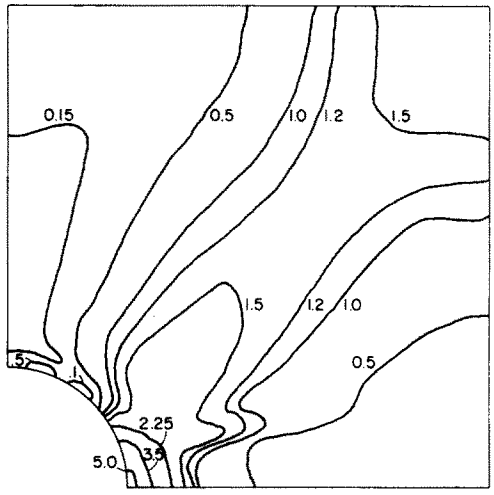

Fig. 12.

Fig. 11. Effective strain rate contours, $\dot{\bar{\varepsilon}}/\dot{\bar{\varepsilon}}_0$. Doubly periodic array—constant uniaxially applied overall strain rate ($L_0/R_0 = 4$, $n = 2$, $U/L_0 = 0.70075$).

Fig. 12. Effective strain rate contours, $\dot{\bar{\varepsilon}}/\dot{\bar{\varepsilon}}_0$. Doubly periodic array—uniaxially applied displacement rate. ($L_0/R_0 = 4$, $n = 5$, $t = 0.0$).

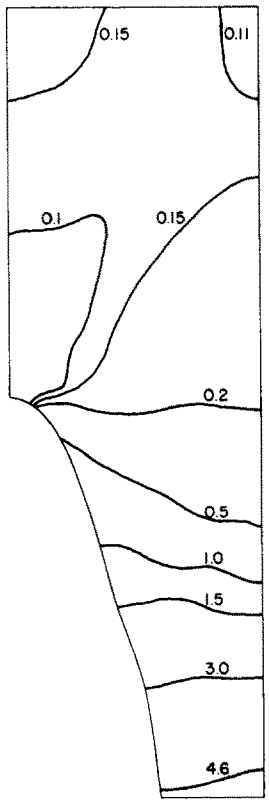

Fig. 13. Effective strain rate, contours, $\dot{\bar{\varepsilon}}/\dot{\bar{\varepsilon}}_0$. Doubly periodic array—constant uniaxially applied overall strain rate ($L_0/R_0 = 4$, $n = 5$, $U/L_0 = 0.952$).

Initially, the deformation is even more concentrated in a narrow band along the diagonal of the unit cell and at the void surface than in the previous cases. A new feature to the contours appeared at this level of creep exponent and was observed as well for higher values of n. A second finger of concentrated deformation, similar to that along the diagonal, was found to extend outwards from the void surface, making an angle of approx. 17° with the x_1 axis. This test was continued until an overall deformation of $U/L_0 = 0.95268$ was reached. The number of iterations required for convergence was found to be greater than for $n = 2$, varying from 8 to 13 per increment. The test was terminated at this stage as fracture was imminent. The magnitude of the lateral displacement rate of the void surface at this stage was 0.112×10^{-13}. The initial value was -0.189×10^{-14}. The uniform nominal traction across the top of the cell is less than 60% of the nominal stress needed to sustain the same uniaxial strain rate in the material without voids. The normalized effective strain rate contours for the final increment of deformation are illustrated in Fig. 13.

The final test in the series of studies on the time dependent finite deformation of the doubly periodic array was for the case $n = 10$. In obtaining the initial solution for this case, the iterative procedure provided the initial solutions for the cases $n = 6$, 7, 8 and 9 as well. The normalized effective strain rate contours for the case $n = 9$ ($t = 0$) is illustrated in Fig. 14. The deformation is extremely localized and concentrated along two bands emanating from the void surface and

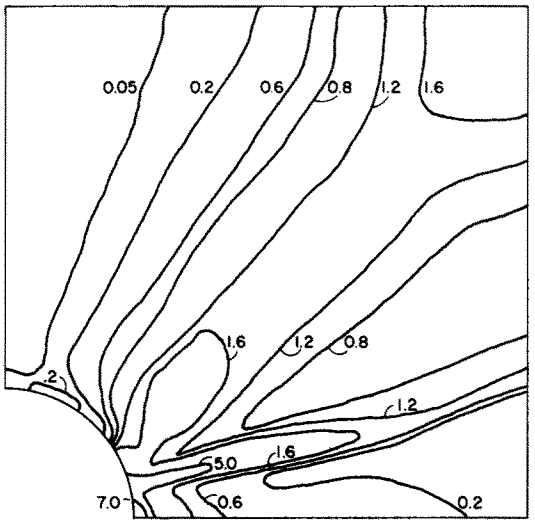

Fig. 14. Effective strain rate contours, $\dot{\bar{e}}/\dot{\bar{e}}_0$. Doubly periodic array—uniaxially applied displacement rate. ($L_0/R_0 = 4$, $n = 9$, $t = 0.0$).

at the intersection of the x_1 axis and the void surface. It appears that the band along the cell diagonal represents nearest neighbor interactions. The second shear band which first became evident for the case $n = 5$ and which is very distinct at $n = 9$, 10 appears to represent the second nearest neighbor interactions.

The result which was of primary interest in this study was the effect of the creep exponent on the extent to which voids interact and the rate at which they coalesce. The response of a doubly periodic array of voids to a constant uniaxially applied strain rate bears some similarity to the response of the necked bar in tension having the same steady creep constitutive behavior. The results of the study of the behavior in the latter case have been previously discussed [29]. In essence, it was demonstrated there that apparent homogeneous deformation persisted despite a condition of material instability which existed during the development of a geometric inhomogeneity. The extent of apparent uniform deformation and the rate of change in strain just prior to fracture were found to be strongly dependent on the creep stress exponent. Now consider the results for the deformational behavior of the void array. Let the initial cell length be denoted as L_0, the initial ligament width along the x_1 axis as D_0, the decrease in D_0 as δ (i.e. $\delta = D_0 - D$, D being the current width), and U as the overall deformation. It then follows for a material without voids, which deforms incompressibly, that

the longitudinal and transverse measures of strain are given by

$$\frac{U}{L_0} = e^{\dot{\epsilon}_{22}t} - 1, \tag{49}$$

$$\frac{\delta}{D_0} = 1 - e^{-\dot{\epsilon}_{22}t} \tag{50}$$

and

$$\frac{\delta}{D_0} = \frac{U}{L_0 + U} \tag{51}$$

this relationship has been plotted in Fig. 15 along with the results for the void growth study. Up to a point, the deviation from apparent homogeneous behavior is not great, at least for the range of creep exponent values which was used in this study. The tendency, in this primary stage, was for the value of δ/D_0 at a particular level of overall strain to decrease with higher values of n. Beyond a point which corresponded to approximately 45% overall strain for this particular void concentration, the deviation from homogeneous behavior increased. The rate at which this occurred was strongly dependent on the value of the creep stress exponent. A conservative estimate of the ductility can be made by extrapolating the curves in Fig. 15 to the point $\delta/D_0 = 1.0$. The following approximate values of the true fracture strain, ϵ_f, were found:

Table 1. Creep fracture strain for doubly periodic array of voids, $L_0/R_0 = 4$

n	ϵ_f
1	1.35
2	1.03
5	0.76
10	0.47

8. SUMMARY

A sufficient amount of evidence exists in support of the fact that failure can occur by the growth and coalescence of voids. The mechanism by which this process occurs at elevated temperatures is not clearly understood. Theories have been proposed to explain cavitation by the stress assisted diffusion of vacancies to the voids or by the time dependent plastic

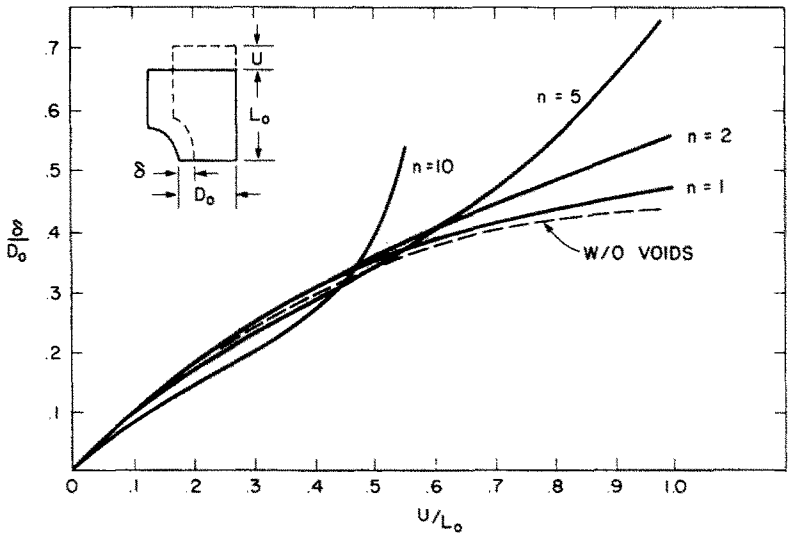

Fig. 15. Relative contraction of the ligament between voids vs the overall engineering creep strain of a doubly periodic array ($L_0/R_0 = 4$).

deformation of the matrix. The work presented here is meant to be a contribution to the latter theory. The approach which was taken here is similar to the early efforts which were taken to study ductile rupture by time independent elastic–plastic deformation; namely, to study first the phenomenon of void interactions for simple uniaxial loading. Certain characteristics of the deformational behavior of the doubly periodic array were found to be similar to the behavior of necked creep tension test specimens. The present work establishes a framework for more comprehensive studies of creep fracture.

An aspect of intergranular fracture which should be examined involves the influence of cracks. Experimental results[31, 32] show that creep fracture sometimes results from the propagation of microcracks along grain boundaries. The large triaxial stresses which exist at the crack tip will cause nearby voids to grow rapidly and will permit the crack to advance by linking with the voids. Obviously a model that contains these features will predict lower and more realistic ductilities than those found in the present study. This was the approach that was taken by Rice and Johnson[22] in their development of a fracture criterion based on the ductile time independent plastic growth of a void in the vicinity of a crack tip. The computational scheme presented in the present work permits a similar study for materials undergoing steady state creep deformation.

Acknowledgements—This work was supported by the National Science Foundation through a Thrust Program on the Application of the Finite Element Method administered by the Center for Materials Research at Stanford. The encouragement and assistance of Prof. D. M. Barnett and Dr. R. L. Mallett is gratefully acknowledged.

REFERENCES

1. G. L. Dunlop, E. Shapiro, D. M. R. Taplin and J. Crane, *Met. Trans.* **4**, 2039 (1973).
2. N. G. Needham, J. E. Wheatly and G. W. Greenwood, *Acta Met.* **23**, 23 (1975).
3. D. A. Kelly, *Acta Met.* **23**, 1267 (1975).
4. R. Raj and M. F. Ashby, *Acta Met.* **23**, 653 (1975).
5. D. Hull and D. Rimmer, *Phil. Mag.* **4**, 673 (1959).
6. G. W. Greenwood, *Phil. Mag.* **8**, 707 (1963).
7. M. V. Speight and J. E. Harris, *Metal Sci. J.* **1**, 83 (1967).
8. J. Weertman, *Met. Trans.* **5**, 1743 (1974).
9. P. W. Davies and B. Wilshire, *Structural Processes in Creep*, p. 34. ISI, London (1961).
10. S. L. Robinson, Ph.D. Dissertation, Stanford University (1972).
11. R. W. Lund and W. D. Nix, *Acta Met.* **24**, 469 (1976).
12. W. Pavinich and R. Raj, *Met. Trans.* **8A**, 1917 (1977).
13. R. J. DiMelfi and W. D. Nix, *Int. J. Solids Structures* **13**, 217 (1976).
14. F. C. Monkman and N. J. Grant, *Proc. ASTM* **56**, 593 (1956).
15. B. Wilshire and P. W. Davies, *J. Inst. Mat.* **90**, 470 (1962).
16. C. K. L. Davies, P. W. Davies and B. Wilshire, *Phil. Mag.* **12**, 827 (1965).
17. P. W. Davies and R. Dutton, *Acta Met.* **14**, 1138 (1966).
18. D. McLean, *Rep. Prog. Phys.* **29**, 1 (1966).
19. E. B. Glennie, *J. Mech. Phys. Solids* **20**, 415 (1972).
20. J. R. Rice and D. M. Tracey, *J. Mech. Phys. Solids* **17**, 201 (1969).
21. F. A. McClintock and A. S. Argon, *Mechanical Behaviour of Materials*, p. 525. Addison Wesley, New York (1966).
22. J. R. Rice and M. A. Johnson, The role of large crack tip geometry changes in plane fracture. In *Inelastic Behaviour of Solids* (Edited by M. F. Kanninen, W. F. Adler, A. R. Rosenfield and R. I. Jaffee), p. 641. McGraw-Hill, New York (1970).
23. D. M. Tracey, Brown University Techn. Rep. No. 34 (1968).
24. A. Needleman, *J. Appl. mech., Trans. ASME* **39**, 964 (1973).
25. G. A. Greenbaum and M. F. Rubenstein, *Nucl. Engng Design* **7**, 379 (1968).
26. W. H. Sutherland, *Nucl. Engng Design* **11**, 269 (1970).
27. O. C. Zienkoewicz and I. C. Cormeau, *Int. J. Num. Meth. Engng* **8**, 821 (1974).
28. I. C. Cormeau, *Int. J. Num. Meth. Engng* **9**, 109 (1975).
29. M. A. Burke and W. D. Nix, *Acta Met.* **23**, (7), 793 (1975).
30. E. P. Timoshenko and J. N. Goodier, *Theory of Elasticity*, Chap. 4, p. 90. McGraw-Hill, New York (1970).
31. H. C. Chang and N. J. Grant, *Trans. AIME* **206**, 544 (1956).
32. N. J. Grant and A. Chaundhuri, Creep and fracture. In *Creep and Recovery*, p. 284. ASM, New York (1975).